Nuclear charge radii of the Te isotopes from muonic atoms

E. B. Shera and M. V. Hoehn
Los Alamos National Laboratory, University of California, Los Alamos, New Mexico 87545

G. Fricke and G. Mallot
Institut für Kernphysik der Universität Mainz, D-6500 Mainz, Federal Republic of Germany
(Received 3 October 1988)

The muonic atom energies of the $2p$-$1s$ and the $3d$-$2p$ transitions were measured with a statistical accuracy of better than ± 70 and ± 40 eV, respectively, for ^{123,124,125,126,128,130}Te. The values for the Barrett equivalent nuclear radii $R_{k,\alpha}$ and for the root-mean-square radii and their differences were calculated first from muonic data alone and second with the addition of published optical data. The latter data provided the radii of ^{120}Te and ^{122}Te isotopes, which were not measured by muonic x rays. A combined analysis of the muonic atom and optical isotope shift data yielded high-precision values of the differences in radii $\Delta R_{k,\alpha}$ (error $< \pm 0.5$ am) and $\Delta \langle r^2 \rangle^{1/2}$ (error $< \pm 0.9$ am) between the neighboring isotopes. The optical constants for the Te line $\lambda = 4049$ Å were determined (including contributions of higher radial moments) to be $F = (509 \pm 120)$ mK/fm^2 and $M = -(104 \pm 63) \times 10^3$ mK. Systematic behavior of the radius differences in neighboring isotopes and isotones of Ba, Xe, Te, and Sn, together with odd-even staggering of the Te isotopes, are discussed in this paper. The $\Delta N = 2$ Te isotope shifts between even-A nuclei decrease nearly linearly with increasing N, which can be explained by a successive decreasing deformation in accordance with the observed systematics. The experimental data for the Te isotopes proved to be in good agreement with even-A Hartree-Fock calculations and with recent Hartree-Fock calculations for odd-A nuclei in which three-body forces are considered. A linear decrease of the nuclear skin thickness with decreasing deformation was observed and is explained by a simple model.

I. INTRODUCTION

The present work is part of a collaborative study involving Los Alamos, Mainz, and Fribourg in which muonic-atom techniques are used to explore charge radii in the region from light to medium-heavy nuclei and in particular to study the influence of the neutron and proton shell structures on nuclear charge radii. It has been found that for neutron shells $N = 20$, 28, and 50,[1-3] the addition of the first two neutrons of a new shell causes a sudden rise of the root-mean-square (rms) radius difference. This behavior is observed to be almost independent of the proton configuration of the nuclei involved. Furthermore, the sequential addition of neutron pairs in the same neutron shell results in an almost linear decrease in the successive radii differences. The small radii differences between the Ba isotopes before the magic neutron number $N = 82$ are consistent with this behavior. The tellurium isotopes, the subject of the present work, can give additional information in this region.

As is well known, optical isotope shifts give information that is complementary to that obtained from muonic atoms: most important, optical data can be obtained for long chains of isotopes including unstable nuclei. However, two isotope shift constants for the specific optical transition in question must be determined before radius differences can be inferred from the optical data. This calibration can be done with the absolute radii deduced from muonic atom x-ray measurements. In this work we determined the optical isotope shift constants for the Te isotopes by comparing our muonic data with optical data from the literature.

The absolute nuclear radii deduced from muonic atoms are so accurate (uncertainty ≈ 1 am), even compared to radii from high-energy elastic electron-scattering experiments (uncertainty ≈ 6–12 am),[4] that these data can readily be used to study systematic effects in differences of radii between neighboring isotones. See, for example, the systematic effects on isotone shifts at $Z = 20$ and 28 measured by muonic atoms.[2] Because changes in radii of isotones are caused by two effects, the charge of the added protons and the proton core polarization, the charge distribution of the added protons must be taken into account before one can obtain information concerning proton core polarization. One is then able to compare the polarization effect of the added protons on the proton core with the neutron polarization effect, the latter being directly given by isotope shifts. If isotone shifts in the $Z = 50$ region follow the systematics observed at $Z = 28$[2] we can expect a large change in radius between Te ($Z = 52$) and Sn ($Z = 50$).

II. APPARATUS AND MEASURED TRANSITION ENERGIES

The muonic x-ray spectra of the six Te isotopes in the present study were obtained at the Los Alamos Meson Physics Facility (LAMPF) muon channel, which provided approximately 10^5 stopped muons per second. The muonic $3d$-$2p$ and $2p$-$1s$ transition energies were mea-

TABLE I. Isotopic composition of the Te targets.

Target \ Isotope	^{120}Te	^{122}Te	^{123}Te	^{124}Te	^{125}Te	^{126}Te	^{128}Te	^{130}Te
^{123}Te	<0.03	1.17	85.40	5.12	1.69	2.56	2.27	1.80
^{124}Te	<0.03	0.12	0.12	93.75	2.31	1.55	1.23	0.92
^{125}Te	<0.01	0.03	0.06	0.28	95.67	2.71	0.76	0.49
^{126}Te	<0.02	<0.02	<0.02	0.05	0.20	98.69	0.81	0.24
^{128}Te	<0.05	<0.05	<0.05	<0.05	<0.05	0.23	99.16	0.61
^{130}Te	<0.02	0.04	0.02	0.02	0.03	0.1	0.3	99.49

sured with a 60-cm^3 Ge(Li) diode. The various Te targets were always studied in sets of four and were permuted among the four target positions periodically to minimize systematic geometrical effects. A detailed description of the Ge(Li) spectrometer and the data-acquisition system has been given in a previous paper.[2]

The first step of the data analysis is to determine the line positions of the muonic x rays and of their accompanying calibration lines. As we are interested in the transition energies of the pure isotopes, the isotopic composition of the targets has been taken into account in the following way. We first analyzed a run with the target combination ^{125,126,128,130}Te. As can be seen from Table I, where the isotopic composition of the targets is given, all contributions of the lighter isotopes ^{123,124}Te may be neglected for these targets. We did a simultaneous fit for the four spectra of these targets, where the relative amplitudes of all contributing isotopes were fixed. This procedure yields the line positions of pure isotopes rather than the positions of the actual lines from the mixed-composition targets. Knowing the relative energy spacing between these heavier isotopes, we can determine the positions of ^{123,124}Te in the same way from runs containing ^{123,124}Te and at least one of the heavier isotopes.

For the odd nuclei ^{123,125}Te (nuclear spin $I=\frac{1}{2}$), the hyperfine splitting due to the magnetic dipole moment and the resulting mixing of nuclear and muonic levels has been calculated with the code MUON2.[5] We used the magnetic moments and known $B(E2)$ values[6,7] for the low-lying nuclear states, as discussed in Sec. III. The relative spacing and amplitudes of the hyperfine components were fixed at the computed values during the fitting procedure.

All these fits were done with the code MYFIT,[8] which uses a rather conventional parametrization of the Ge(Li) line shape. This line shape is the sum of a Gaussian and several asymmetry contributions for the high- and low-energy sides of the peak. These asymmetry functions result from a convolution of exponential and Gaussian functions. They have the form $\exp(2ax)\times[1\pm\mathrm{erf}(x+a)]$, where x is the normalized channel number, i.e., the energy, and a is responsible for the shape (for details see

TABLE II. Energy calibration sources and their γ-ray energies (Refs. 10 and 11).

Isotope	γ-ray energy (keV)
^{203}Hg	279.197(1)
^{137}Cs	661.600(3)
^{46}Sc	889.277(3)
^{24}Na	1368.633(6)
	2754.030(14)
^{56}Co	3201.954(14)
	3253.417(14)
	3272.998(14)
	3451.154(13)
	3547.925(61)
^{88}Rb	3218.483(49)
	3486.473(56)
	4035.500(400)

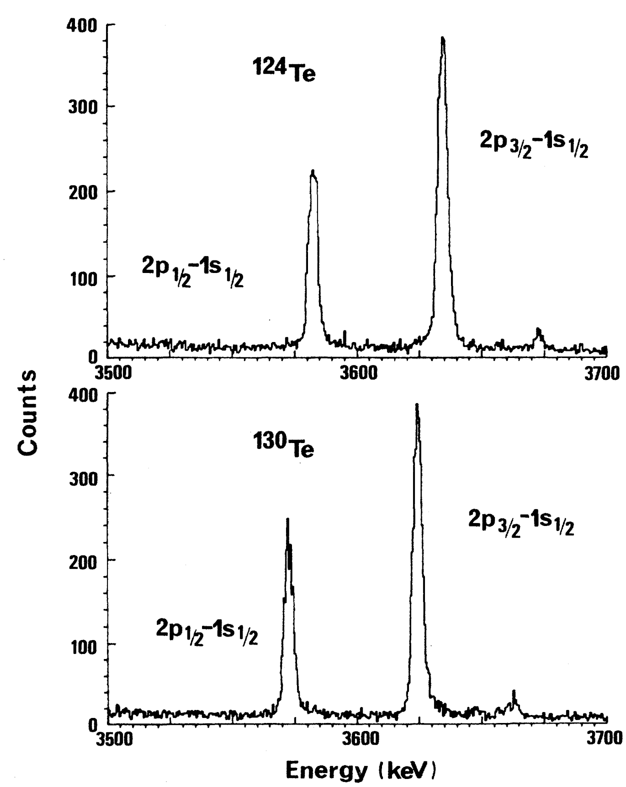

FIG. 1. Spectra from the muonic $2p_{3/2}$-$1s_{1/2}$ and $2p_{1/2}$-$1s_{1/2}$ transitions for ^{124}Te and ^{130}Te. The isotope shift is almost 20% of the fine-structure splitting. The FWHM is 4.8 keV.

TABLE III. Experimental transition energies for the $2p_{3/2}$-$1s_{1/2}$, $2p_{1/2}$-$1s_{1/2}$, $3d_{3/2}$-$2p_{1/2}$, $3d_{5/2}$-$2p_{3/2}$, and the $3d_{3/2}$-$2p_{3/2}$ transitions. The listed error includes the uncertainties of the calibration lines (Table II) and the statistical uncertainty in the location of the line centroids.

	Transition energies (keV)				
Isotope	$2p_{3/2}$-$1s_{1/2}$	$2p_{1/2}$-$1s_{1/2}$	$3d_{3/2}$-$2p_{1/2}$	$3d_{5/2}$-$2p_{3/2}$	$3d_{3/2}$-$2p_{3/2}$
^{123}Te	3637.191(71)	3585.249(68)	1106.653(30)	1061.645(30)	1054.693(46)
^{124}Te	3634.446(68)	3582.502(62)	1106.419(30)	1061.475(30)	1054.481(40)
^{125}Te	3633.532(69)	3581.595(65)	1106.451(30)	1061.503(30)	1054.544(41)
^{126}Te	3630.882(68)	3579.011(61)	1106.240(30)	1061.357(30)	1054.375(40)
^{128}Te	3627.578(68)	3575.716(62)	1106.095(30)	1061.274(30)	1054.257(40)
^{130}Te	3624.486(67)	3572.652(62)	1105.971(30)	1061.158(30)	1054.160(40)

Hughes and Wu[9]). The peak position is defined as the center of gravity of the area of the peak from the 20% point up to the maximum of the line. This method of defining peak positions reduces the influence of line-shape asymmetries.

The energy calibration of the Ge(Li) spectrometer in the region of the $2p$-$1s$ transition energies of tellurium (3.6 MeV) is difficult because of the low intensities of radioactive calibration lines in this energy region. For this reason, we split the calibration into a lower (0.3–2.7 MeV) and an upper energy region (2.7–4 MeV). Before and after the muonic experiment the Ge(Li) spectrometer was calibrated with γ rays from 0.3–4 MeV (Table II). During the experiment calibration lines in the low-energy region were stored in proportion to the instantaneous muon beam intensity, as discussed in Ref. 2.

As the four Te spectra measured in any one run have identical calibration, the *energy differences* between such isotopes can be determined more accurately than can the absolute energies. For the same reason, energies derived from spectra of the same run are not independent. To get a consistent set of energies and their differences, we have treated all line positions of all runs together. This procedure gives the energies, the calibration parameters, and the relevant error matrix. From this information the energy differences and their uncertainties have been computed.

To extend the calibration from the lower energy region to the region of interest around 3.7 MeV, we used the calibration spectra extending up to 4 MeV, taken before and after the muonic runs. A linear function is assumed to describe any possible difference between the calibration before the run and the calibration during the run. This procedure was tested in the energy region from 0.3–2.7 MeV with numerous calibration lines. The resulting χ^2 of 1.1/degree of freedom indicates that this as-

TABLE IV. Isotope shift values for the $2p_{3/2}$-$1s_{1/2}$ (23-11) and $2p_{1/2}$-$1s_{1/2}$ (21-11) transition energies (keV). Only statistical uncertainties are given.

^{123}Te	−51.942										
23-11	40										
^{124}Te	2.747	54.689									
21-11	38	31									
^{124}Te	−49.196	2.745	−51.944								
23-11	37	26	25								
^{125}Te	3.654	55.596	0.907	52.851							
21-11	43	37	35	33							
^{125}Te	−48.282	3.659	−51.030	0.914	−51.937						
23-11	39	30	29	24	34						
^{126}Te	6.238	58.180	3.491	55.434	2.584	54.520					
21-11	38	32	27	25	34	29					
^{126}Te	−45.632	6.309	−48.380	3.564	−49.287	2.650	−51.870				
23-11	37	27	25	19	33	24	24				
^{128}Te	9.533	61.475	6.786	58.730	5.879	57.816	3.295	55.166			
21-11	41	35	31	30	36	31	31	29			
^{128}Te	−42.329	9.613	−45.076	6.868	−45.983	5.954	−48.567	3.304	−51.862		
23-11	38	29	27	22	33	25	27	22	30		
^{130}Te	12.597	64.539	9.850	61.794	8.943	60.880	6.359	58.230	3.064	54.926	
21-11	42	37	32	31	37	33	31	30	34	31	
^{130}Te	−39.237	12.705	−41.984	9.960	−42.891	9.046	−45.475	6.396	−48.770	3.092	−51.834
23-11	39	30	28	23	34	26	20	22	30	24	29
	^{123}Te	^{123}Te	^{124}Te	^{124}Te	^{125}Te	^{125}Te	^{126}Te	^{126}Te	^{128}Te	^{128}Te	^{130}Te
	21-11	23-11	21-11	23-11	21-11	23-11	21-11	23-11	21-11	23-11	21-11

sumption is consistent with the measurements. A deviation from linearity should occur only if the change of the line positions, due to drift, become significant compared to the linear regions of the apparatus. Since the maximum observed shift was two analog-to-digital converter (ADC) channels during the entire experiment (one week) the assumption seems well justified. The assumed linearity of the apparatus between 3.2 and 3.7 MeV was confirmed with several calibration lines (Table II) as well as with a high-accuracy pulser.[1]

Using these two assumptions, we developed the computer code CONFIT,[12] which adjusts the transition energies to all measured line positions and gives, for each run, the calibration parameters for the energy region from 3.2 to 3.7 MeV and the associated error matrix. The $3d$-$2p$ transitions (1.0–1.1 MeV) were analyzed in the same way.

Figure 1 shows, as an example, the $2p_{3/2}$-$1s_{1/2}$ and $2p_{1/2}$-$1s_{1/2}$ spectra for ^{124}Te and ^{130}Te. The shift in the energies due to the different radii (approximately 10 keV) is readily apparent compared to the $2p$ fine-structure splitting of approximately 52 keV. The experimental results are given in Tables III and IV with the least-squares adjusted isotope shift values for the $2p_{3/2}$-$1s_{1/2}$, $2p_{1/2}$-$1s_{1/2}$ and the $3d_{3/2}$-$2p_{1/2}$, $3d_{5/2}$-$2p_{3/2}$, $3d_{3/2}$-$2p_{3/2}$ transition energies.

An impression of the consistency of the line fitting and the energy calibration can be obtained from a plot of the $2p$ fine-structure splitting energies of each isotope (Fig. 2) as independently deduced from the $2p$-$1s$ and the $3d$-$2p$ transitions. The $\Delta 2p$ values are generally in good agreement and, as expected in view of the finite-size effect, display a gradual decrease in energy with increasing A.

The averaged $2p$-$1s$ transition energies from previous measurements by Kast *et al.*[13] are in agreement with our measurements, which are an order of magnitude more precise. However, their individual $2p_{3/2}$-$1s_{1/2}$ and $2p_{1/2}$-$1s_{1/2}$ transition energies only agree with our results within two standard deviations.

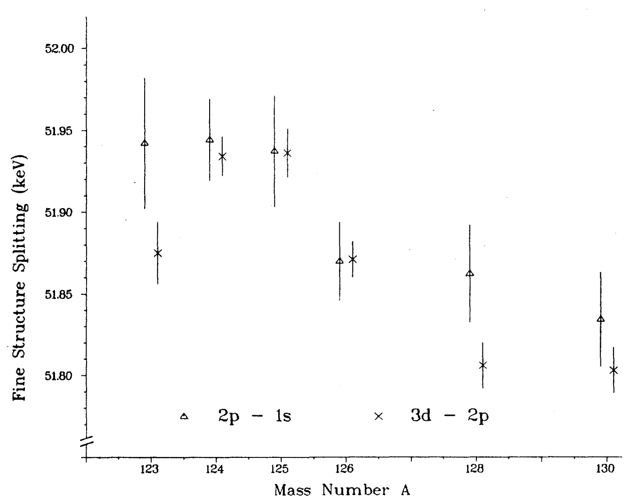

FIG. 2. Fine-structure splitting energies (keV) of the muonic $2p$ level for the different tellurium isotopes from the measured $2p$-$1s$ ($\triangle$) and $3d$-$2p$ ($\times$) transitions.

III. NUCLEAR CHARGE RADII

A. Nuclear charge parameters from muonic transition energies

To determine the nuclear radial moments from muonic-atom transition energies, one typically solves the Dirac equation with the two-parameter Fermi nuclear charge distribution (in the following equations we use the notation of Ref. 1)

$$\rho_N(r)=\rho_0\{1+\exp[(r-c)/a]\}^{-1} \tag{1}$$

and adjusts the half-density radius c and the skin-thickness parameter t ($t=4\ln 3a$) to reproduce the measured $2p$-$1s$ and $3d$-$2p$ transition energies. Barrett[14] has shown that the radial moment

$$\langle r^k e^{-\alpha r}\rangle=4\pi\int_0^\infty \rho_{\rm nucl}(r) r^k \exp(-\alpha r) r^2 dr \tag{2}$$

can be determined "model independently" from muonic transition energies, provided k and α are properly adjusted to the muon potential difference of the transition in question:

$$r^k e^{-\alpha r} \sim [V_\mu^i(r)-V_\mu^f(r)] \ . \tag{3}$$

Equation (2) follows from considerations of the energy shift of a muonic transition due to a change of the spherical nuclear charge distribution $\Delta\rho_{\rm nucl}$, which, in first-order perturbation theory, is given by

$$\Delta E=4\pi\int_0^\infty \Delta\rho_{\rm nucl}(r)[V_\mu^i(r)-V_\mu^f(r)]r^2 dr \ . \tag{4}$$

The Barrett moment can be expressed in terms of the Barrett equivalent nuclear charge radius $R_{k,\alpha}$ of a homogeneously charged sphere, which reproduces the transition energy in question and has the dimension of a length, by the relationship

$$3[R_{k,\alpha}]^{-3}\int_0^{R_{k,\alpha}} r^k e^{-\alpha r} r^2 dr=\langle r^k e^{-\alpha r}\rangle \ . \tag{5}$$

With the computer code MUON2,[5] we have solved the Dirac equation numerically using the two-parameter Fermi distribution and applied quantum-electrodynamic (QED) and nuclear polarization (NP) corrections. The code MUON2 (Ref. 5) is a modified version of codes MUON and RURP.[15]

The NP corrections include the isoscalar and isovector contributions for giant resonance multipoles $0\le L\le 3$. The strength of each electric multipole was concentrated in a single resonance state whose energy[5] and strength was determined by the full sum rules. These "high-lying states" corrections have a smooth A dependence; therefore, only the values for the lightest and the heaviest Te isotope are shown (Table V). The quadrupole contributions to the low-lying 2^+ states have been included using the known energies and $B(E2)$ values of these states.[16] For the odd isotopes ^{123}Te and ^{125}Te one has to calculate the hyperfine structure and the nuclear polarization due to the low-lying states in one procedure. Therefore, the single NP value given in Table VI for each isotope contains both effects and their interference. Owing to the use of a model for the transition charge densities and to other

TABLE V. Nuclear polarization contribution from the isoscalar (S) and isovector (V) giant resonances (GR) of different electric multipoles $0 \le L \le 3$ (high-lying states). Because of their smooth A-dependence only the values for the lightest ^{123}Te and the heaviest ^{130}Te isotopes are given.

GR	Isotope	Energy (MeV)	$B(EL)$ (e^2b^L)	$1s_{1/2}$ (eV)	$2p_{1/2}$ (eV)	$2p_{3/2}$ (eV)
$E0$ S	123	14.903	0.0219	358	7	3
	130	14.751	0.0209	345	6	3
$E0$ V	123	27.146	0.0164	175	4	2
	130	26.649	0.0174	188	4	2
$E1$ V	123	15.535	0.287	699	126	111
	130	15.335	0.303	742	134	118
$E2$ S	123	12.668	0.322	221	38	34
	130	12.436	0.310	215	37	33
$E2$ V	123	26.140	0.213	107	16	14
	130	25.662	0.225	114	17	15
$E3$ S	123	22.119	0.160	42	6	5
	130	21.714	0.154	41	6	5
$E3$ V	123	39.411	0.123	25	3	3
	130	38.691	0.130	27	4	3
Sum	123			1627	200	172
	130			1672	208	179

calculational assumptions, the NP corrections[17] have an uncertainty of about 30%.

The corrections arising from the low-lying states can differ considerably from one isotope to another, especially between even and odd ones. For example, the NP correction applied to the d-p transitions for ^{123}Te is almost 125 eV larger than the correction for the other Te isotopes (Table VII). If the level structure of an isotope is not well known, as is frequently the case for odd isotopes, the error of the NP corrections may be larger than the experimental error in the measured transition energies. The effect of NP uncertainties on the extraction of optical constants will be discussed further in Sec. III B. The uncertainties of the QED corrections (Table VII) are estimated to be about 20 eV.[18]

After the two parameters c and t have been adjusted to the measured transition energies, the values for α and k can be directly calculated from the muon potentials. Be-

TABLE VI. Nuclear polarization corrections calculated from the low-lying states, the excitation energies, and the $B(E2)$ values are given. Only the uncertainties for the $B(E2)$ values of ^{123}Te are included since they are large compared to the others. The listed values for the odd isotopes include the hyperfine splitting calculated with $\mu_I(123) = -0.7359\mu_k$ and $\mu_I(125) = -0.888\,28\mu_k$ (Ref. 16).

	Excitation energy (keV)	I^π	$E(B2)$ (e^2b^2)	NP corrections $1s_{1/2}$ (eV)	$2p_{1/2}$ (eV)	$2p_{3/2}$ (eV)
^{123}Te	158.99	$\frac{3}{2}^+$	0.020(4)			
	440.00	$\frac{3}{2}^+$	0.260(20)	703	519	569
	505.34	$\frac{5}{2}^+$	0.360(30)			
	687.95	$\frac{5}{2}^+$	0.004			
^{124}Te	602.73	2^+	0.568(5)	615	384	397
	1325.52	2^+	0.019	20	8	8
^{125}Te	443.50	$\frac{3}{2}^+$	0.186			
	463.39	$\frac{5}{2}^+$	0.158	512	355	379
	671.42	$\frac{5}{2}^+$	0.130			
	729.30	$\frac{5}{2}^+$	0.003			
^{126}Te	666.34	2^+	0.478	520	305	311
	1420.17	2^+	0.004	4	2	2
^{128}Te	743.30	2^+	0.377	408	225	227
^{130}Te	839.40	2^+	0.300	319	165	164

TABLE VII. Theoretical corrections used in the analysis for the various muonic transitions. Note NP corrections for the d-p transitions are almost 124 eV larger for ^{123}Te than for all other isotopes.

Isotope	$2p_{1/2}$-$1s_{1/2}$	$2p_{3/2}$-$1s_{1/2}$	$3d_{3/2}$-$2p_{1/2}$	$3d_{5/2}$-$2p_{3/2}$	$3d_{3/2}$-$2p_{3/2}$
	NP corrections (eV)				
^{123}Te	1610	1589	710	732	732
^{124}Te	1676	1691	585	572	570
^{125}Te	1600	1596	556	552	552
^{126}Te	1669	1691	501	481	481
^{128}Te	1646	1673	428	400	401
^{130}Te	1618	1648	362	333	332
	QED corrections for ^{126}Te (eV)[a]				
	$2p_{1/2}$-$1s_{1/2}$	$2p_{3/2}$-$1s_{1/2}$	$3d_{3/2}$-$2p_{1/2}$	$3d_{5/2}$-$2p_{3/2}$	$3d_{3/2}$-$2p_{3/2}$
VP[b]	26 497	27 327	8624	7885	7794
QED[c]	−1513	−1418	−55	−150	−150
Sum (QED)[d]	24 984	25 909	8569	7735	7644
Sum[e]	26 653	27 600	9070	8216	8125

[a]Because of the smooth A dependence, values for only a single isotope are given.
[b]Electronic vacuum polarization of order $\alpha(Z\alpha)$ and $\alpha^2(Z\alpha)$.
[c]Higher-order corrections.
[d]Sum of VP and QED.
[e]Sum of sum(QED) and NP corrections.

cause of the model independence of the Barrett radial moments, the choice of the Fermi distribution does not affect the results expressed in terms of the Barrett radii. The model independence can be estimated by varying the nuclear skin-thickness parameter t by 10%. This is approximately the largest change of t observed for one isotopic chain by elastic electron scattering on the isotopes ^{40}Ca and ^{48}Ca.[19] The result for the Barrett radius $R_{k,\alpha}$ ($2p_{1/2}$-$1s_{1/2}$) changes only by 0.2 am for Te. This value is less than the experimental error and the uncertainties of NP corrections. The results for the tellurium charge parameters are given in Table VIII, where we used, for all Te isotopes, the same k and α values for a given transition. This procedure is justified because the variation of k and α for the different isotopes is negligible.

The original approximation of Ford and Wills[20] which parametrized the information contained in each transition energy by the radial moment $\langle r^k \rangle$ of the charge distribution, although more model dependent than the Barrett approximation, is also more transparent. To give a better understanding for the measured quantities, we list in Table IX the Ford-Wills k values for the five transi-

TABLE VIII. Nuclear charge parameters (fm) deduced from muonic x rays. Only statistical uncertainties are listed. The Barrett parameters k,α are given for each transition.

Barrett parameters:

$2p_{3/2}$-$1s_{1/2}$ (23-11): $k=2.2178$, $\alpha=0.1141$ (1/fm)
$3d_{3/2}$-$2p_{1/2}$ (33-21): $k=2.3680$, $\alpha=-0.0461$ (1/fm)
$3d_{5/2}$-$2p_{3/2}$ (35-23): $k=4.2969$, $\alpha=0.1429$ (1/fm)

Isotope	c	t	$\langle r^2\rangle^{1/2}$	$\langle r^4\rangle^{1/4}$	$R_{k,\alpha}$ 23-11	$R_{k,\alpha}$ 33-21	$R_{k,\alpha}$ 35-23
^{123}Te	5.496 78	2.397	4.7158	5.0637	6.0296	6.1476	6.1952
			0.0006	0.0025	0.0002	0.0017	0.0022
^{124}Te	5.534 67	2.334	4.7200	5.0606	6.0382	6.1498	6.1950
			0.0006	0.0025	0.0002	0.0016	0.0022
^{125}Te	5.567 25	2.267	4.7194	5.0522	6.0407	6.1456	6.1884
			0.0006	0.0025	0.0002	0.0016	0.0022
^{126}Te	5.562 68	2.298	4.7270	5.0635	6.0489	6.1569	6.2006
			0.0006	0.0025	0.0002	0.0016	0.0022
^{128}Te	5.593 01	2.253	4.7331	5.0647	6.0590	6.1626	6.2045
			0.0006	0.0025	0.0002	0.0016	0.0022
^{130}Te	5.616 04	2.223	4.7393	5.0676	6.0684	6.1691	6.2098
			0.0006	0.0025	0.0002	0.0016	0.0022

TABLE IX. The Ford and Wills parameter k for the five measured transitions.

Transition	k
$2p_{1/2}$-$1s_{1/2}$	1.657
$2p_{3/2}$-$1s_{1/2}$	1.660
$3d_{3/2}$-$2p_{1/2}$	2.612
$3d_{3/2}$-$2p_{3/2}$	3.509
$3d_{5/2}$-$2p_{3/2}$	5.510

tions measured in this work. Because the radial information from the $2p_{3/2}$-$1s_{1/2}$ and the $2p_{1/2}$-$1s_{1/2}$ transitions is almost identical, in Table VIII we list only the $R_{k,\alpha}$ deduced from the transitions with the better statistics.

For comparison with optical isotope shift experiments, we have used the parameters c and t of a Fermi charge distribution as determined by the $3d$-$2p$ and $2p$-$1s$ transition energies. These parameters and the second and fourth radial moments are also listed in Table VIII. The quoted error is only statistical; however, one should keep in mind that these Fermi charge parameters are not model independent at the high level of accuracy presented in the present measurements.

B. Root-mean-square radii, their differences and optical isotope shift measurements

As discussed in the preceding section, the various muonic transitions specify different radial moments (Table IX). To extract the rms radius differences, one needs at least two independent radial moments to determine the radius c and the skin thickness t of the Fermi two-parameter charge distribution. The sensitivity of the Barrett radii for the $2p$-$1s$ transition energy is high ($1/C_z = dE/dR_{k,\alpha} \cong -300$ eV/am), and therefore the corresponding radii can be determined very precisely (Table VIII). In the case of the $3d$-$2p$ transition the sensitivity is much lower ($1/C_z = -8$ eV/am). Also the uncertainty of the $2p$ NP correction is considerable. For these reasons our determination of the Barrett radii for the $3d$-$2p$ transition is significantly less certain than for the $2p$-$1s$ transition.

In this work we made two separate analyses of our data. First we used the $2p$-$1s$ and $3d$-$2p$ transitions to determine the charge distribution parameters (Table VIII) from muonic measurements alone as described in Sec. III A. In a second (combined) analysis we included the results of optical isotope shift measurements on the Te isotopes, as described in the following paragraphs.

The optical isotope shifts $\delta\nu^{AA'}$ are a linear function of the radius differences $\lambda^{AA'}$

$$\delta\nu_{\rm exp}^{AA'} = F\lambda^{AA'} + M(A'-A)/(A'A) ,$$

where

$$\lambda^{AA'} = \delta\langle r^2\rangle^{AA'} + c_2/c_1\,\delta\langle r^4\rangle^{AA'} + \cdots , \qquad (6)$$

$$M = N + S ,$$

and

$$N = \nu m_e/m_p .$$

In these relations F is the difference in electron density at the nucleus for the two levels of the transition, N is the normal mass shift, S is the specific mass shift, ν is the frequency of the transition, m_e is the electron mass, m_p is the proton mass, and the c_i are Seltzer's coefficients.[21] For Te the ratio of the Seltzer coefficients $c_2/c_1 = -6.4\times10^{-4}$, and the higher radial moments can make a significant contribution to the isotope shift, especially if the $\delta\langle r^2\rangle$ term happens to be small for a pair of isotopes. For example, the contribution of the higher moments is about 6% for $\lambda^{124,125}$.

Before proceeding we have the problem of combining the data from the several published optical isotope shift measurements on Te, namely those of Kuhn and Turner,[22] Lecordier and Helbert,[23] and Lecordier.[24] Older measurements with larger errors were not includ-

TABLE X. Optical isotope shift data $\delta\nu_{\rm exp}^{AA'}$ (mK) from the measurements of Kuhn *et al.* (Ref. 22) and Lecordier *et al.* (Refs. 23 and 24) are listed. Least-squares adjusted values projected onto the $\lambda=4049$ Å line are used in the analysis.

	Kuhn *et al.* $\lambda=4049$	Lecordier *et al.* $\lambda=4049$	$\lambda=5450$	$\lambda=5479$	$\lambda=4007$	Adjusted $\lambda=4049$
$^{120-122}$Te	22.70					22.70
	1.20					1.20
$^{122-123}$Te	−0.60	−0.70			−1.30	−0.85
	0.70	0.60			0.80	0.41
$^{122-124}$Te	21.50	20.70	−2.80	6.57	21.20	20.78
	0.40	0.30	0.20	0.20	0.40	0.22
$^{124-125}$Te	−1.40	−0.80			−0.90	−1.01
	0.70	0.50			0.50	0.37
$^{124-126}$Te	17.30	18.56	−2.50	5.90	19.10	18.27
	0.40	0.30	0.20	0.20	0.40	0.20
$^{126-128}$Te	16.70	16.70	−2.30	5.03	17.60	16.73
	0.40	0.30	0.20	0.20	0.40	0.20
$^{128-130}$Te	14.50	14.70	−2.00	4.28	15.60	14.72
	0.50	0.30	0.20	0.20	0.40	0.22

TABLE XI. Nuclear charge parameters c, t, and rms radii (fm) from a simultaneous analysis of muonic x-ray energies and optical isotope shift data. δrms (am) and $\delta R_{k,\alpha}$ (am) are the deviations from pure muonic results compared to the simultaneous analysis. For ^{120}Te and ^{122}Te, only optical isotope shift data are available. Only statistical errors are given. Barrett parameters for the transition $2p_{3/2}$-$1s_{1/2}$ (23-11) are $k=2.2178$ and $\alpha=0.1141$ (1/fm).

	c	t	rms	δrms $\mu-(\mu+\text{opt.})$	$R_{k,\alpha}$ 23-11	$\delta R_{k,\alpha}$ $\mu-(\mu+\text{opt.})$
^{120}Te			4.705			
^{122}Te			4.713			
^{123}Te	5.514 35	2.358	4.7142	+1.6	6.0295	+0.1
			0.0005		0.0002	
^{124}Te	5.531 97	2.340	4.7202	−0.2	6.0382	0.0
			0.0005		0.0002	
^{125}Te	5.545 55	2.316	4.7213	−1.9	6.0408	−0.1
			0.0004		0.0002	
^{126}Te	5.563 85	2.295	4.7269	+0.1	6.0489	0.0
			0.0004		0.0002	
^{128}Te	5.593 34	2.253	4.7331	0.0	6.0590	0.0
			0.0004		0.0002	
^{130}Te	5.622 03	2.209	4.7388	+0.5	6.0683	+0.1
			0.0005		0.0002	

ed. The measurements, from four different optical spectral lines, were transferred to one spectral line with the help of a King plot.[25] The King plot compares the measured isotope shifts, normalized by the factor $AA'/(A'-A)$, for two different spectral transitions. In such a plot the data points should form a straight line, as follows from King's assumption that for a given element and a given spectral line the factors F and M are constant. Thus all optical tellurium isotope shift measurements from four different spectral lines could be transferred to the $\lambda=404.9$ nm spectral line by a least-squares fitting procedure. The results, with errors, are given in Table X.

As we have discussed muonic data yield values for Barrett equivalent radii [Eq. (5)], while the dependence of the optical data on charge radius is given by Eq. (6). To combine or compare these two kinds of data requires some knowledge of the form of the nuclear charge distribution. One can take the approach of using the c,t for a Fermi distribution fitted to the muonic data, in combination with the optical data to determine, via King plot, the optical parameters F and M.

However, to make the best use of the available data and to determine the correct errors for the derived quantities, it is convenient to combine both muonic and optical measured data in a single fitting procedure. As input data we used the muonic $2p$-$1s$ and $3d$-$2p$ transition energies (Table III) and the adjusted optical isotope shifts $\delta_\nu^{AA'}$ (Table X) to fit the nuclear charge parameters c and t and the optical constants F and M for the entire tellurium isotope chain simultaneously (Table XI). As mentioned, a major advantage of this procedure is to get the correct error matrix, taking into account the errors from all the input data, which then allows us to calculate the radial moment differences up to the fourth moment and their errors in a consistent way (Table XII and XIII). However, one should keep in mind that these results depend on the assumption of a Fermi two-parameter charge distribution. Without additional experimental information about the shape of the charge distribution, such as from electron scattering, there is no truly model-independent method of combining both muonic and optical data sets.

Our King plot of muonic and optical data is shown in Fig. 3. The data points are the pure muonic data on the x axis, while the y values are given by optical isotope

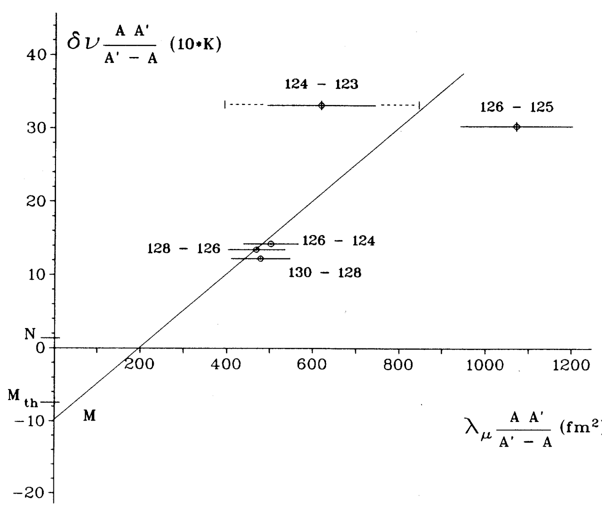

FIG. 3. King plot of optical isotope shift data for the $\lambda=4049$ Å line vs muonic $\Delta\langle r^2\rangle + c_2/c_1\langle r^4\rangle$ values. The straight line is determined by a simultaneous fit of muonic and optical data, $F=509\pm120$ mK/fm², and $M=-(104\pm63)\times10^3$ mK. The extended (dashed) error of the isotope pair $^{124\text{-}123}$Te stems from the uncertainties of the ^{123}Te $B(E2)$ values. M_{th} was calculated by Bauche (Ref. 26).

TABLE XII. Radius differences from a simultaneous analysis of muonic x-ray energies and optical isotope shift data. Only statistical uncertainties are given. The values given for ^{122}Te and ^{120}Te are from optical data alone.

	rms radius differences (am)				
	^{123}Te	^{124}Te	^{125}Te	^{126}Te	^{128}Te
^{124}Te	6.1				
	0.7				
^{125}Te	7.1	1.1			
	0.3	0.7			
^{126}Te	12.7	6.6	5.5		
	0.6	0.2	0.6		
^{128}Te	18.9	12.8	11.8	6.2	
	0.6	0.5	0.5	0.3	
^{130}Te	24.6	18.5	17.5	11.9	5.7
	0.9	0.9	0.8	0.7	0.4
Δrms(^{122}Te-^{120}Te)=8.0					
Δrms(^{124}Te-^{122}Te)=7.2					

	Barret radius differences $\Delta R_{k,\alpha}(2p_{3/2}\text{-}1s_{1/2})$ (am), $k=2.2178$, $\alpha=0.1141$ (1/fm)				
	^{123}Te	^{124}Te	^{125}Te	^{126}Te	^{128}Te
^{124}Te	8.7				
	0.2				
^{125}Te	11.2	2.6			
	0.3	0.2			
^{126}Te	19.4	10.7	8.1		
	0.3	0.3	0.2		
^{128}Te	29.4	20.8	18.2	10.0	
	0.4	0.4	0.3	0.3	
^{130}Te	38.8	30.1	27.6	19.4	9.4
	0.6	0.5	0.5	0.4	0.3

shifts alone. The straight line is the result of our combined optical and muonic analysis, which is a simultaneous fit to the measured muonic transition energies and the measured optical isotope shifts as mentioned above, rather than a fit to the $\delta\langle r^2\rangle^{AA'}+c_1/c_2\delta\langle r^4\rangle^{AA'}$ of the pure muonic analysis. Thus the line in Fig. 3 is not a fit to the displayed data points. The slope of the line is determined principally by the odd isotopes ^{123}Te, ^{125}Te for which muonic and optical data are not in a good agreement. The errors given in Fig. 3 are taken from Table XII, whereas the relatively large error for $^{124\text{-}123}$Te comes from the large uncertainties of the NP corrections, which are due to the large error for the $B(E2)$ values of ^{123}Te compared to ^{125}Te and the other isotopes.

In discussing the deviation of the odd isotopes, one might question the completeness and reliability of the available $B(E2)$ values; however, a reexamination of these data is beyond the scope of the present paper. We should perhaps comment that a shift of the $^{124\text{-}123}$Te point in Fig. 3 towards the $^{126\text{-}125}$Te point seems more likely

TABLE XIII. Differences of the fourth radial moments from a simultaneous analysis of muonic x-ray energies and optical isotope shift data. Only statistical uncertainties are given. For ^{126}Te$\langle r^4\rangle^{1/4}=5.063$ fm.

	$\Delta\langle r^4\rangle^{1/4}$ (am)				
	^{123}Te	^{124}Te	^{125}Te	^{126}Te	^{128}Te
^{124}Te	4.0				
	2.7				
^{125}Te	2.3	-1.7			
	1.1	2.7			
^{126}Te	5.5	1.5	3.2		
	2.5	1.0	2.3		
^{128}Te	7.0	3.0	4.7	1.5	
	2.6	2.0	2.0	1.2	
^{130}Te	8.0	3.9	5.7	2.5	1.0
	3.2	3.3	2.4	2.5	1.5

than the other way around, because of the larger uncertainties in the $B(E2)$ values for ^{123}Te. The result would be in a somewhat smaller mass shift and improved agreement with the value calculated by Bauche[26] of $M_{\rm th}=-75$ mK.

Before discussing the interpretation of the results of Sec. IV, it is desirable also to consider the radii of the neighboring Sn, Xe, and Ba isotopes. To study the systematic behavior of nuclear radii one can use either the precisely known Barrett radii $R_{k,\alpha}$ or the more conventional rms radii. The Barrett radii, however, can be measured only for stable isotopes, whereas by the optical isotope shift method one can measure differences of rms radii—even for unstable isotopes—by laser-spectroscopy techniques. Combining both methods one can get absolute rms radii for long isotope chains. If one adds to these data the information about radii differences between isotones, which can be measured only by muonic atoms, it is possible to study the systematic behavior for chains of isotopes and isotones. Furthermore, if independent measurements for a closed loop of isotope and isotone shifts are available, one can readily check the consistency of the measurements.

To deduce the rms radii from an optical shift measurement, one has to know the two optical constants F and M and the rms radius for one isotope, as outlined in Sec. III B. The following information for Ba, Xe, and Sn has been used (the contribution of the higher radial moments, $\langle r^4\rangle$ and $\langle r^6\rangle$ have not been taken into account).

Ba: Shera *et al.*[27] and Kunold *et al.*[28] determined from muonic x-ray measurements on the Ba isotopes for the 553.5-nm BaI line the optical constants $F=(3035\pm260)$ MHz fm^{-2} with $M=(47\pm103)$ GHz and $\langle r^2\rangle^{1/2}$ (^{138}Ba)=4.832 fm (values taken from Shera *et al.*). With these values and the optical isotope measurements compiled by Heilig[29] one can compute the rms radii for the long chain of isotopes from ^{122}Ba up to ^{146}Ba.

Xe: In his Diplomarbeit, Hennemann[30] found from an analysis of his muonic atom data on the stable Xe isotopes, together with the optical isotopes shift measurement by Borghs *et al.*[31] for the Xe line $\lambda=605.1$ nm, the values $F=(0.63\pm0.09)$ GHz fm^{-2}, $M=(-972\pm52)$ GHz, and $\langle r^2\rangle^{1/2}(^{132}\text{Xe})=4.782$ fm.

Sn: For the tin isotopes the optical values given by Heilig,[29] $F=(3.3\pm0.5)$ GHz fm^{-2} and $M=(98\pm70)$ MHz for the $\lambda=286.3$ nm transition, together with the rms radius for $^{120}\text{Sn}\langle r^2\rangle^{1/2}=4.646$ fm from elastic electron scattering data[32] (which included older muonic x-ray data[33]), give access to all rms radii from ^{108}Sn to ^{124}Sn.

The determination of the optical constants F and M and the rms radius for one isotope for each element is based on previously published data. A more refined evaluation of these quantities, including new data,[34,35] will be given in a forthcoming publication.

IV. INTERPRETATION OF RESULTS

In the region between $N=20$, 28, and 50, almost all Barrett radii for stable isotopes are now known from muonic atom measurements by a collaboration of Los Alamos and the universities of Mainz and Fribourg,[1,2,3,36,37] although for some of the elements the data are still unpublished. On the basis of these data several observations can be made. These observations are summarized in the following.

(a) At the beginning of a new neutron shell, a dramatic increase of the radius occurs. The sequential addition of neutron pairs in the same shell results in an almost linear decrease in the successive isotope shifts. Toward the end of the shell, the isotope shifts can even become negative.

(b) It is apparent that the isotope shifts are nearly independent of the proton configuration of the nuclei involved. This is true even for magic proton configurations; for example, the $^{58}_{26}$Fe-$^{56}_{26}$Fe and $^{60}_{28}$Ni-$^{58}_{28}$Ni isotope shifts are identical within their errors (Ref. 2). The change in the nuclear charge radius is primarily determined by the shell of the added neutrons, whereas the influence of the proton configuration is not very significant. This is especially remarkable when one considers that the charge radius is, after all, given by the proton distribution of the nucleus.

(c) At the end of the neutron shells $N=28$ and 50 one observes a slightly but systematically larger shift for the isotopes of the lighter elements. This effect represents a small deviation from the independence of the isotope shift from the proton configuration as mentioned above.

These previous findings are listed for comparison with the present results for the tellurium isotopes as given in Fig. 4. One sees that the rms radii differences show a slow linear decrease from Δrms($^{122\text{-}120}$Te)=8 am to Δrms($^{130\text{-}128}$Te)=6 am, which is in accordance with the general observation (a). However, the isotope shifts are still positive, in contrast to the trend seen as the $N=28$ shell closure is approached[3] and also for Sr, Rb, Kr, and Br as the $N=50$ shell is approached.

To explain the change in the rms radii between neighboring isotopes, one can use the model of a uniformly charged deformed nucleus

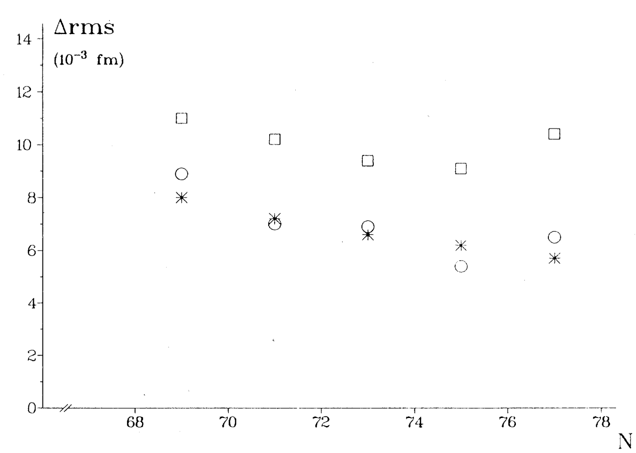

FIG. 4. Differences in nuclear charge rms radii of the even Te isotopes upon the addition of two neutrons: ∗, experiment; □, droplet model with deformation; ○, spherical Hartree-Fock calculations with deformation (see Table XIV).

$$\delta\langle r^2\rangle_{\rm exp}=\delta\langle r^2\rangle_{\rm sph}+\langle r^2\rangle_{\rm sph}5/4\pi\delta\langle\beta^2\rangle \ . \tag{7}$$

The first term accounts for the radius change of the spherical part of the nucleus, whereas the second term is related to the quadrupole deformation β of the nucleus. The terms are usually called the volume and the shape effects, respectively. In principle, deformations of all orders contribute, but in practice the quadrupole deformation β_2 alone will be used because it is expected to dominate and for most nuclei only the $B(E2)$ values are known. The β_2 values, Table XIV, are derived from the measured $B(E2)$ values according to the following formula:[41]

$$\langle\beta_2^2\rangle=B(E2)[4\pi/(3zR_0^2)]^2 \ . \tag{8}$$

Friedrich *et al.*[39] have calculated the $\delta\langle r^2\rangle_{\rm sph}$ term of this formula by the spherical Hartree-Fock (HF) method, using G_σ Skyrme forces. The second term is determined by the variation in the deformation β_2 as given in Table XIV. These compared results for the differences of the rms radii between neighboring even-even Te isotopes show a nearly perfect agreement with the experimental values (Fig. 4).

The results from the droplet model[40] (DM) for the radius differences (Fig. 4) are systematically 3–4 am too high, because of the larger $\delta\langle r_0^2\rangle$ of this model, but show a similar variation with A due to the deformation contribution. This comparison of the present data with the spherical HF and DM predictions involves radii differences. If one considers absolute radii the comparisons are less favorable, even if the influence of deformation on the radii is included empirically (Table XIV).

We have performed density-dependent HF calculations using the method of Negele and Rinker,[38] assuming axially symmetry nuclear deformation and using the density matrix expansion (DME) effective Hamiltonian and the pairing approximation described in Ref. 38. The DME method is appealing compared to the use of Skyrme forces because it is based on realistic two-body effective interaction rather than a purely phenomenological potential. The absolute rms radii from these deformed HF calculations are in excellent agreement with experiment, reproducing the measured values for the light Te isotopes almost within the errors of the measurements (Table XIV). A similar remarkable agreement between the DME calculations and experiment has been reported in a rather different class of nuclei, namely the transitional Os-Pt isotopes.[42]

It is evident that a variation of the deformation should be related to a change in the skin thickness t of the nuclear charge distribution. The measurements of the $2p$-$1s$ and $3d$-$2p$ muonic transitions allow us to determine the skin thickness t as well as the radius parameter c of the Fermi two-parameter model (Table XI). The value for the four isotopes ^{124,126,128,130}Te are plotted on a display of t vs β_2 in Fig. 5.

The apparent linearity of the plots suggests an extrapolation to $\beta_2=0$, which leads to a skin thickness of about $t=1.9$ fm. A formal justification of this linear extrapolation follows from the model of a uniformly charged axially symmetric quadrupole-deformed nucleus. Its charge distribution is given by Kopfermann[43] as

$$\rho(r)=\begin{cases}\rho_0, & r<b\\ \rho_0\cdot(1-[(r-b)/(a-b)]^{1/2}), & b<r<a \ ,\\ 0, & r>a \ ,\end{cases} \tag{9}$$

where a,b are the axes of the deformed ellipsoid. From the following well-known relations:

$$\beta_2\sim\sqrt{B(E2)}\sim Q_0\sim(a^2-b^2) \ . \tag{10}$$

With the two assumed charge parameters $t=0.8(a-b)$ and $R=(a+b)/2$ one gets for the skin thickness $t=\sqrt{9/5\pi}R\beta_2$. With the simple liquid-drop model $R=R_0A^{1/3}$ follows the linear relation

$$t=\sqrt{9/5\pi}R_0A^{1/3}\beta_2 \ . \tag{11}$$

The experiment yields $t_{\rm exp}=m\beta+t_0$ with $m=2.813$ fm and $t_0=1.877$ fm, which gives $R_0=0.74$ fm, in agreement with other isotope shifts near the closure of a neutron shell.[44] The value of $t_0\approx1.9$ fm may be regarded as the skin thickness of an idealized, totally spherical nucleus.

One can ask the question: what is the smallest skin thickness observed for an actual nucleus? One should expect to find this for doubly magic nuclei, for example, in the calcium isotope ^{48}Ca ($\beta_2=0.1$) with $t=2.26$ fm as measured by elastic electron scattering.[19] This value can

TABLE XIV. Comparison of the measured rms radii for the even Te isotopes with deformed Hartree-Fock calculations from Negele *et al.* (Ref. 38), spherical Hartree-Fock calculations from Friedrich *et al.* (Ref. 39), and the spherical droplet mode (Ref. 40). The spherical values are corrected for β_2 deformation deduced from B(E2) values (Ref. 16).

		rms radii (fm)			
Te	μ+opt. exp.	Deformed HF	β_2	Spherical HF $+\beta_2$	Spherical droplet $+\beta_2$
120	4.705	4.707	0.180	4.682	4.717
122	4.713	4.713	0.174	4.691	4.728
124	4.720	4.722	0.164	4.698	4.739
126	4.727	4.734	0.150	4.705	4.748
128	4.733	4.746	0.132	4.710	4.757
130	4.739	4.754	0.117	4.717	4.767

be compared with the smallest skin thickness observed for a Te isotope, which occurs as expected in the isotope nearest the $N=82$ closed shell, ^{130}Te ($\beta_2=0.12$) with $t=2.21$ fm. The observations are consistent. The t values of the ^{134,136,138}Ba isotopes measured from muonic atoms given by Shera *et al.*[27] lead to a $t_0=1.95$ fm, a value also consistent with the result from the Te isotopes.

The systematic behaviors of the rms radii described in observations (a) and (c) above, which were found at the closure of the $N=50$ neutron shell,[3] are also apparent for Te and neighboring elements at $N=82$. As an illustration, the measured differences of the rms radii ($\Delta N=2$) for the even Te isotopes are displayed in Fig. 6 together with the isotope shifts of Ba, Xe, and Sn. They all show a linear decrease approaching the neutron number $N=82$ [effect (a)], and the rms values are systematically larger for lower Z elements [effect (c)].

Figure 7 shows the isotope shifts ($\Delta N=2$) and isotone shifts ($\Delta Z=2$) for Te, Sn, Xe, and Ba plotted against the neutron and proton numbers N and Z, respectively. The size of the shifts is displayed by the width of the arrows; the arrows point in the direction of increasing radius. The polarization of the proton core by the added neutrons, the isotope shifts, shows an almost monotonic decrease approaching $N=82$. A slight deviation from monotonic behavior occurs for the last two added neutrons before the closure of the neutron shell. These neutrons generate a small increase of the radius difference, due perhaps to the admixture of neutron states of the next shell (Fig. 7). The first two added neutrons in the new shell $^{140\text{-}138}$Ba produce a dramatic increase in the radius difference, as expected from the systematics [see observation (a)].

One must remember that the ^{50}Sn-^{52}Te-^{54}Xe-^{56}Ba isotone shifts arising from the addition of two protons can be understood as the result of two effects: first, by adding the charge of these protons into the $1g_{7/2}$ orbit, and second, by the polarization of the proton core. There is a large increase of the rms radius for the first two added protons in the $1g_{7/2}$ shell, i.e., between the Sn and Te isotones. Adding further protons results in a linear decrease in the isotone shifts; see, for example, the isotones with 70, 72, or 74 neutrons. Also, the isotone shifts between Sn and Te decrease linearly as the neutron number becomes larger. These observations display essentially the same systematics as those outlined for isotope shifts. These results for the Sn and Xe isotopes are preliminary, and a more quantitative comparison will be made in a forthcoming publication.[45]

The two odd isotopes ^{123}Te and ^{125}Te exhibit the usual odd-even staggering effect. A staggering parameter $\gamma(A)$ can be defined[1]

$$\gamma(A+1)=2[R(A+1)-R(A)]/[R(A+2)-R(A)]\ , \tag{12}$$

with A even and R the rms radius. γ is normally smaller

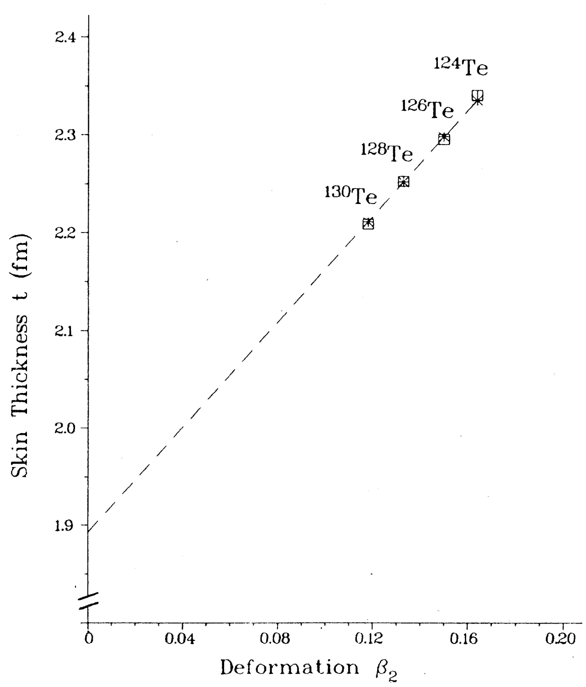

FIG. 5. Deformation parameter β_2 from $B(E2)$ values plotted against skin thickness t of the adjusted Fermi distribution from a simultaneous fit of muonic and optical data □ and calculated values * (see text).

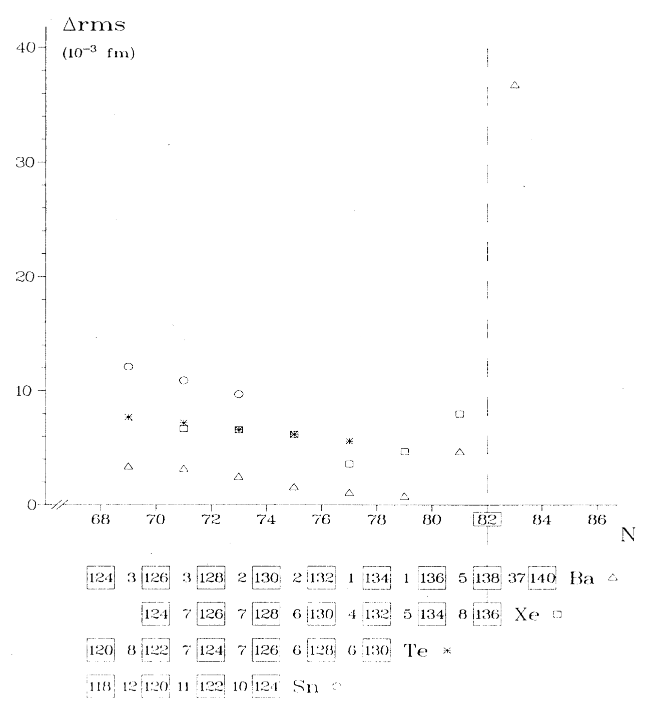

FIG. 6. Differences in rms nuclear charge radii upon addition of two neutrons for the barium, △; the xenon, □; the tellurium, *; and the tin, ○ isotopes. It is apparent that Δ rms values decrease as the magic neutron number $N=82$ is approached and that the values are systematically larger for lower Z elements. The well-known large increase after $N=82$ is seen for barium.

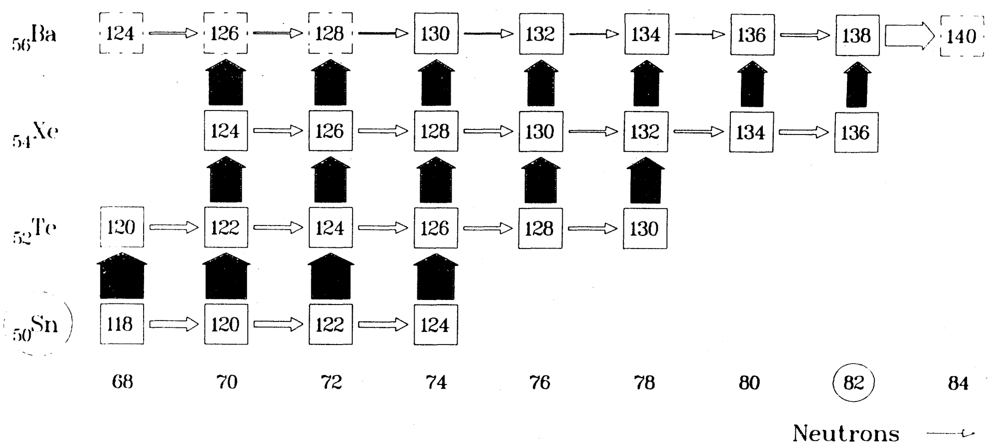

FIG. 7. The increase of the rms radii between neighboring even-even isotopes (horizontal arrows) and isotones (vertical arrows) is represented by the width of the arrows in a Z-N plot. The figure gives an overall impression of the systematic behavior of the isotone and isotope shifts. The references for these data are given in Sec. III.

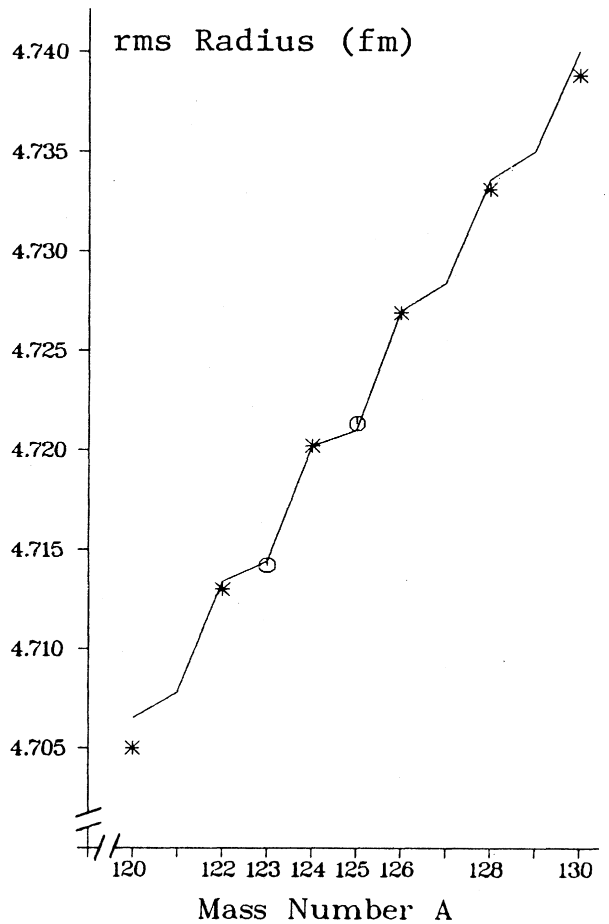

FIG. 8. The measured rms radii for the Te isotopes—indicated by different symbols for odd and even nuclei—are plotted for comparison with the calculations of Zawischa applying three-body forces. For convenience the theoretical values are connected by lines.

than 1, which means that the increase of the rms radius due to the added odd neutron is smaller than one-half the difference between the even N neighbors. The experimental values are

$$\gamma(^{123}\mathrm{Te})=0.31\pm0.14$$

and (13)

$$\gamma(^{125}\mathrm{Te})=0.33\pm0.18\ .$$

Recent Hartree-Fock-Bogoliubov calculations from Zawischa,[46]

$$\gamma_{\mathrm{th}}(^{123}\mathrm{Te})=0.18$$

and (14)

$$\gamma_{\mathrm{th}}(^{125}\mathrm{Te})=0.24\ ,$$

show good agreement with the experiment. These calculations included a three-body δ force and used the parameter set developed for the Sn isotopic chain, with the single exception that the strength of the two-particle interaction was reduced by a factor of 2. The results of these calculations are displayed in Fig. 8 (connected by lines) together with the experimental values (distinctive symbols are used to distinguish odd and even isotopes). The good agreement with experiment, including the odd-even staggering, is evident. We also note that the pairing-plus-quadrupole model calculations, published some time ago by Reehal and Sorensen,[47] are not in good agreement with our experimental values.

ACKNOWLEDGMENTS

The authors wish to acknowledge the contributions of Th. Hennemann, L. A. Schaller, L. Schellenberg, R. M. Steffen, H. D. Wohlfahrt, and J. D. Zumbro to this work by their valuable assistance and discussions. The work was supported by the U.S. Department of Energy and by the Bundesministerium für Forschung und Technologie of the Federal Republic of Germany.

[1]E. B. Shera, E. T. Ritter, R. B. Perkins, G. A. Rinker, L. K. Wagner, H. D. Wohlfahrt, G. Fricke, and R. M. Steffen, Phys. Rev. C **14**, 731 (1976).

[2]H. D. Wohlfahrt, E. B. Shera, M. V. Hoehn, Y. Yamazaki, and R. M. Steffen, Phys. Rev. C **23**, 533 (1981).

[3]G. Fricke *et al.*, in *Proceedings of the 4th International Conference on Nuclei Far From Stability, Helsingor, 1981,* European Organization for Nuclear Research Report RD/504, 1981, p. 1600.

[4]W. Reuter, G. Fricke, K. Merle, and H. Miska, Phys. Rev. C **26**, 806 (1982).

[5]Y. Tanaka (private communication); the program MUON2 (unpublished) based on G. Rinker, codes MUON and RURP.

[6]T. Tamura, Z. Matumoto, K. Miyano, and S. Ohya, Nucl. Data Sheets **29**, 499 (1980).

[7]T. Tamura, Z. Matumoto, and M. Ohshima, Nucl. Data Sheets **32**, 547 (1981).

[8]G. Mallot, MYFIT.

[9]V. Hughes and C. S. Wu, *Muon Physics* (Academic, New York, 1979).

[10]R. G. Helmer, R. C. Greenwood, and R. J. Gehrke, Nucl. Instrum. Methods **155**, 189 (1978).

[11]R. C. Greenwood, R. G. Helmer, and R. J. Gehrke, Nucl. Instrum. Methods **159**, 465 (1979).

[12]G. Mallot, CONFIT.

[13]J. W. Kast, S. Bernow, S. C. Cheng, D. Hitlin, W. Y. Lee, E. R. Macagno, A. M. Rushton, and C. S. Wu, Nucl. Phys. **A169**, 62 (1971).

[14]R. C. Barrett, Phys. Lett. **33B**, 388 (1970).

[15]G. A. Rinker, Comput. Phys. Commun. **16**, 221 (1978).

[16]T. Tamura, Z. Matumoto, K. Miyano, and S. Ohya, Nucl. Data Sheets **29**, 499 (1980).

[17]G. A. Rinker and J. Speth, Nucl. Phys. **A306**, 397 (1978).

[18]G. A. Rinker and R. M. Steffen, At. Data Nucl. Data Tables **20**, 143 (1977).

[19]H. J. Emrich, Ph.D. thesis, Universität Mainz, 1983.

[20]K. W. Ford and J. G. Wills, Phys. Rev. **185**, 1429 (1969).

[21]E. C. Seltzer, Phys. Rev. **188**, 1916 (1969).

[22]H. G. Kuhn and R. Turner, Proc. R. Soc. London, Ser. A **265**, 39 (1961).

[23]R. Lecordier and J. M. Helbert, Physica **94C**, 125 (1978).

[24]R. Lecordier, Phys. Lett. **72A**, 327 (1979).

[25]W. H. King, *Isotope Shifts in Atomic Spectra* (Plenum, New York, 1984).

[26]J. Bauche (private communication); see R. Lecordier, Phys. Lett. **72A**, 327 (1979).

[27]E. B. Shera, H. D. Wohlfahrt, M. V. Hoehn, and Y. Tanaka, Phys. Lett. **112B**, 124 (1982).

[28]W. Kunold, M. Schneider, L. M. Simons, J. Wüst, and R. Abela, Z. Phys. A **313**, 11 (1983).

[29]K. Heilig, Hyperfine Interact. **24**, 349 (1985).

[30]Th. Hennemann, Ph.D. thesis, Universität Mainz Report KPH 2/84, 1984.

[31]G. Borghs, P. DeBisschop, R. E. Silverans, M. Van Hove, and J. M. Van den Cruyee, Z. Phys. A **299**, 11 (1981).

[32]J. R. Ficence, L. A. Fajardo, W. P. Trower, and I. Sick, Phys. Lett. **42B**, 213 (1972).

[33]R. Engfer, H. Schneuwly, J. L. Vuilleumier, H. K. Walter, and A. Zehnder, At. Data Nucl. Data Tables **14**, 509 (1974).

[34]E. B. Shera *et al.* (unpublished).

[35]Th. Hennemann *et al.* (unpublished).

[36]H. D. Wohlfahrt, E. B. Shera, M. V. Hoehn, Y. Yamazaki, G. Fricke, and R. M. Steffen, Phys. Lett. **73B**, 131 (1978).

[37]L. Schellenberg, B. Robert-Tissot, K. Käser, L. A. Schaller, H. Schneuwly, G. Fricke, S. Glückert, G. Mallot, and E. B. Shera, Nucl. Phys. **A333**, 333 (1980).

[38]J. W. Negele and G. Rinker, Phys. Rev. C **15**, 1499 (1977).

[39]J. Friedrich and N. Voegler, Nucl. Phys. **A459**, 10 (1986).

[40]W. D. Myers and K.-H. Schmidt, Nucl. Phys. **A410**, 61 (1983).

[41]D. M. Stacay, Rep. Prog. Phys. **29**, 171 (1966).

[42]W. Reuter, E. B. Shera, M. V. Hoehn, F. W. Hersman, T. Milliman, J. M. Finn, C. Hyde-Wright, R. Lourie, B. Pugh, and W. Bertozzi, Phys. Rev. C **30**, 1465 (1984).

[43]H. Kopfermann, *Nuclear Moments* (Academic, New York, 1958).

[44]E. W. Otten, in *Treatise on Heavy-Ion Physics,* edited by D. Bromley (Plenum, New York, in press), Vol. 8.

[45]G. Fricke *et al.* (unpublished).

[46]D. Zawischa, U. Regge, and R. Stapel, Phys. Lett. B **185**, 299 (1987); D. Zawischa (private communication).

[47]B. S. Reehal and R. A. Sorensen, Nucl. Phys. **A1261**, 385 (1971).